3-3 Ionospheric Storm and Variation of Total Electron Content

3-3-1 Observations of TEC Disturbances with GEONET —TEC Storm and SED—

MARUYAMA Takashi, MA Guanyi, and NAKAMURA Maho

Two extreme ionospheric events were analyzed as phenomena in which ionospheric total electron content (TEC) was significantly enhanced. The first event occurred on November 6, 2001, associated with a magnetic storm. TEC derived from a nationwide GPS receiver network (GEONET) reached 200 TEC units at a lower latitude (27° N) and 100 TEC units at a higher latitude (45° N). These values are double the quiet-day averages. This enhanced TEC had been primarily caused by the prompt penetration of a magnetospheric electric field into lower latitudes associated with a geomagnetic disturbance. The second event was storm enhanced density (SED) that occurred on November 8, 2004. TEC became enhanced at higher latitudes after sunset and it reached 100 TEC units, higher than the daytime maximum on a quiet day at the same latitude and 20 times higher than at the same local time on a quiet day. In addition to a penetrating magnetospheric electric field, a disturbance dynamo electric field may have played a major role in the formation of SED moving in the WNW direction.

Keywords
Ionospheric total electron content, TEC storm, SED, Magnetospheric disturbances, Disturbance dynamo

1 Introduction

Technologies based on radio waves make our lives more convenient and enrich various aspects of our social system. One major characteristic of radio waves is their ability to propagate over long distances. Since HF radio waves reach as far as the opposite side of the globe through repeated reflection between the ionosphere and ground surface, HF communication and broadcasting used to be the key means of distributing and exchanging information overseas. As the application of satellites has become a permanent part of society, radio waves at higher frequencies that propagate through the ionosphere have opened up a diverse range of applications. Yet, the ionosphere is not a perfect transparent medium for satellite radio waves. In particular, radio waves in the UHF band, such as those transmitted from GPS satellites, and at lower frequencies are significantly affected by propagation delays, fluctuations in signal strength, and other effects. The magnitude of these effects largely depends on the state of a continually varying ionosphere.

Variations in ionospheric electron density can be roughly divided into two kinds: regular and sudden. Regular variations have distinct characteristics of periodicity, such as solar activity having a cycle of approximately 11 years, seasonal variations associated with the earth's revolution around the sun, and daily variations, which are therefore somewhat easy

to model (as reported in References[1][2]). In contrast, rapid changes in solar activity such as solar flares could induce a series of disturbances in the terrestrial upper atmosphere driven by a magnetic storm, resulting in sudden variations in the ionosphere[3]–[7]. This phenomenon is called an "ionospheric storm." Ionospheric storms in which the electron density diminishes are called "negative storms," and those in which the electron density enhances are called "positive storms." The way that ionospheric storms behave vary significantly; for example, a positive storm might turn into a negative storm as time progresses; either a positive storm or a negative storm might develop at one time; or a positive storm and a negative storm might develop simultaneously at different latitude. Generally, ionospheric storms are electron density disturbances on a global scale, but rarely is a sharp rise in electron density observed in a narrow region associated with magnetic storms. This phenomenon is called SED (storm enhanced density), whereby the electron density leaps several times or even 20 times higher than normal at around sunset. SEDs are closely related to daytime positive disturbances. Because decreases in critical frequency foF_2 in negative storms reduce the maximum usable frequency for HF communication, active research using ionosonde has long been conducted. Today, positive storms take on growing importance in connection with radio propagation delays in the ionosphere, such as those transmitted from GPS satellites. Ionospheric delays of satellite radio waves are proportional to the total electron content (TEC), or the integrated value of electron density along the propagation path from the satellite to the receiver. Figure 1 shows the relation between the TEC and propagation delays in the case of GPS L_1 and L_2 signals, where 1 TEC unit refers to 1×10^{16} electrons/m^2. Regular variations or sudden disturbances might cause TEC to vary from several TEC units up to 200 TEC units.

In recent years, TEC observed by GPS satellites has been widely used for ionospheric studies as well as foF_2 observed by ionosondes. One reason for this impetus is that GPS receivers are easier to install than ionosondes and afford more observation stations. Although foF_2 and TEC behave similarly as each being a measure of an ionospheric variation, both are not identical measures. Therefore, we should use both measures in a complementary manner for detailed analysis. Another essential function of ionosondes is their observation of ionospheric height. The photo-chemical process has a significant bearing on ionospheric variations, and largely depends on height. Moreover, since ionospheric height variations directly reflect atmospheric and plasma dynamics, the ionospheric height offers a key parameter in elucidating the mechanism of ionospheric storm development, along with foF_2 and TEC.

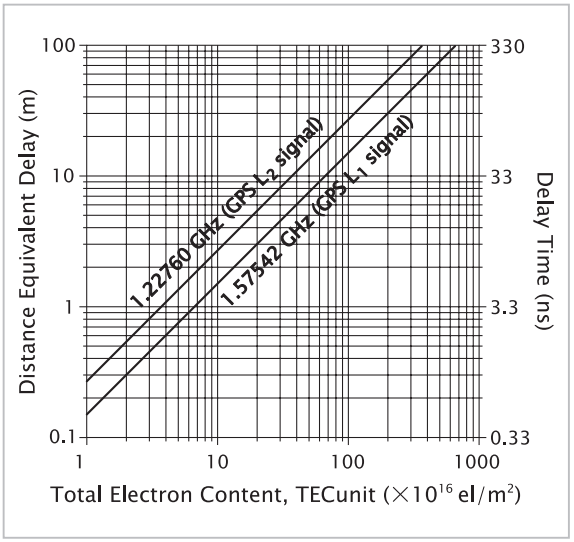

Fig.1 *Relation between the ionospheric propagation delays of GPS L_1 and L_2 signals and TEC*

This paper deals with two extremely significant events involving positive ionospheric variations having immense importance to space weather, with reference to TEC maps derived from a dual-frequency GPS receiver network (GEONET: GPS Earth Observation Network) built by the Geospatial Information Authority of Japan (GSI), as well as foF_2 and h_mF_2 (maximum electron density height) derived from four ionosonde observatories in Japan. The first event is the ionospheric storm that occurred on November 6, 2001. This

storm was quite exceptional in exhibiting a record increase in TEC, but not a particularly large event in terms of foF_2. This event therefore acquired the name "TEC storm." The second event is SED observed after sunset on November 8, 2004. Ionospheric storms usually develop in an intricate complexity of three factors; one increasing electron density, the second decreasing it, and the third sustaining such effects. The next chapter briefly reviews the mechanism of ionospheric storms. After describing the dataset employed, the two events are discussed in detail.

2 Mechanism of Ionospheric Storm

Negative storms are caused by changes in atmospheric composition driven by energy having been injected into polar regions during a magnetic storm. A thermospheric atmosphere having its composition changed propagates toward lower latitudes in the form of traveling atmospheric disturbances (TADs)[8]. Changes in the composition are represented by an increase in the $[N_2]/[O]$ ratio and inducing an increase in the recombination coefficient of ionospheric plasma, thus resulting in decreased electron density. In the initial stage of a TAD, an equatorward wind intensifies (equatorward surge) to push up the plasma along inclined geomagnetic field lines. If this phenomenon occurs in the daytime, the electron density increases since the electron loss rate is lower at higher altitudes. In this way, a positive storm may precede a negative storm, though this largely depends on the time period during which the equatorward surge occurred. Another cause of positive ionospheric disturbances is the plasma having been uplifted ($\mathbf{E}\times\mathbf{B}$ drift) in the direction perpendicular to the magnetic field ($\mathbf{B}$) by an eastward electric field ($\mathbf{E}$). The electron loss rate reduces at higher altitudes as in the case of wind effect. When this happens during daylight hours, the electron density increases. This eastward electric field originates from broadly two sources. One is an intensified magnetospheric convection electric field penetrating into lower latitudes[9]; the other a disturbance dynamo induced by changes in thermospheric general circulation driven by energy having been injected into a polar region[10][11].

In the case of actual ionospheric storms, a number of complicated factors may interact with one another to enhance disturbances or even cancel one another[3]. Forbes et al.[12] and Forbes[13] attempted to separate multiple disturbance sources by using data collected from a set of ionosondes arranged in the meridian. However, the principal sources of disturbance may generally change with the lapse of time, with the significance of each disturbance process also varying from event to event, thus making it a laborious task to fully identify the sources of disturbances.

foF_2 is the most fundamental of all parameters that characterize an ionospheric storm, but inadequate by itself to gain complete insight into the complexities of disturbances. Even if the ionospheric F-layer is uplifted to higher altitudes by an eastward electric field or equatorward thermospheric neutral wind, it might cause foF_2 to increase or decrease depending on the local time or the rate of rising height. As explained by Rishbeth[14], the outflow of plasma from the ionosphere to the plasmasphere could reduce NmF_2 (NmF_2 [m^{-3}] = 1.24×10^{10} (foF_2 [MHz])^2) under certain circumstances, but the degree of this effect varies greatly depending on the neutral atmospheric wind and $\mathbf{E}\times\mathbf{B}$ drift. The fall in foF_2 caused by the rising maximum electron density height (hmF_2) of the F-layer is a consequence of plasma being redistributed along the geomagnetic field line and changes in the ionospheric height profile. The plasmasphere has a function of drawing out ionospheric plasma in the daytime and then replenishing the ionosphere with plasma at nighttime. The effect of rising foF_2 caused by rising hmF_2 is associated with a decrease in the electron recombination rate and the progress of ionization in the bottomside ionosphere. The increase or decrease in foF_2 is ultimately determined depending on which of the two conflicting effects is domi-

nant. Likewise, foF_2 may rise or fall even when the F-layer height has been lowered by a downward **E**×**B** drift driven by a westward electric field or a poleward thermospheric neutral wind. Rising foF_2 results from a deformed ionospheric height profile, whereas sagging foF_2 stems from an increase in the electron recombination rate. The rise in foF_2 is transient and soon overcome by the effect of recombination in the bottom-side ionosphere, with foF_2 beginning to decrease.

The method of observing TEC using radio waves transmitted from GPS satellites has recently been widely adopted, thereby encouraging research on ionospheric storms by using TEC. Essentially, TEC behaves in a manner similar to foF_2 in the course of an ionospheric storm, though not necessarily matched. When foF_2 is varied upon the redistribution of plasma along the geomagnetic field line, for example, the integral value of TEC does not show a major change, because redistribution alone neither recombines nor generates plasma. On the other hand, when foF_2 falls as a result of an increase in the recombination rate, TEC will follow it. Since TEC is an integrated parameter over the ionosphere to the plasmasphere, TEC is slower to respond to changes in the electron loss rate in the lower ionosphere when compared to foF_2, and TEC and foF_2 exhibit different temporal changes. Thus, analyzing two observed values that differ in behavior should greatly aid in interpreting ionospheric storms.

3 Data

GEONET built by GSI consists of more than 1,200 GPS receivers, allowing TEC between a satellite and receivers to be estimated using a signal transmitted on two frequencies. Among various methods of estimation proposed to date, we have employed the method developed by Ma and Maruyama[15]. According to this method, the coverage of the receiver network (piercing points at which satellite radio waves pass an ionospheric height) was divided into 32 cells (2×2° in latitude/longitude), and with TEC being estimated using the least square fitting method on the assumption of constant vertical TEC in each of these cells. While this process of TEC estimation is based on the fact that radio waves propagating at two different frequencies undergo different propagation delays in the ionosphere, it simultaneously solves inter-frequency biases (or differences in instrumental delay between two frequencies within the electronic circuit) unique to satellites and receivers. TEC for the 32 cells was evaluated every 15 min from a 24-hr data set, assuming that the satellite and receiver biases remain unchanged during 24 hours. Based on the resultant TEC data, a time (LT) and latitude TEC map was produced from the 24-hr TEC data (24×4×32) by the spherical harmonic functional fitting method. A map of differences between quiet and disturbed days created from this TEC map visualizes ionospheric storms as seen by TEC.

As shown in Fig. 2, ionosondes were in operation at the four observatories located at Wakkanai, Kokubunji, Yamagawa, and Okinawa, with each offering an ionogram every 15 min. Table 1 summarizes the locations of these observatories. Besides foF_2, transmission

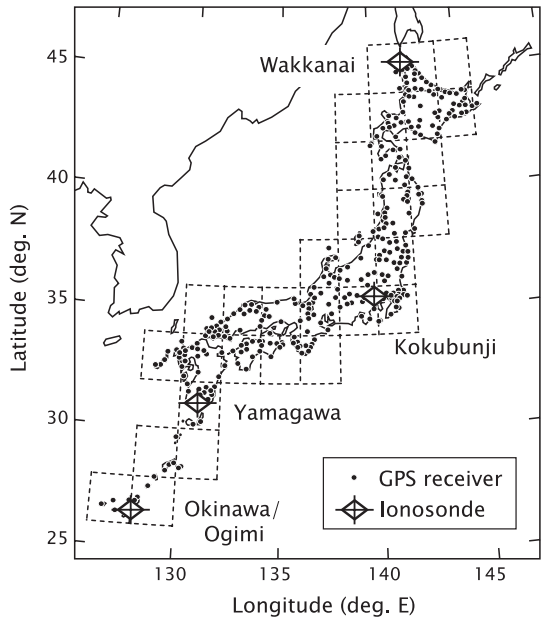

Fig.2 *Distribution of GEONET receivers used to determine TEC*

Table 1 Location of Ionosondes

Station	Latitude (° N)	Longitude (° E)	Magnetic inclination (°)
Wakkanai	45.39	141.69	59.8
Kokubunji (Tokyo)	35.71	139.49	49.3
Yamagawa	31.20	130.62	44.5
Okinawa/Ogimi	26.68	128.16	37.8

factor $M(3000)F_2$ was scaled from the ionograms. Using $M(3000)F_2$, ionospheric height h_mF_2 was calculated by the following relational expression[17] produced by correcting an equation based on work done by Shimazaki[16] to allow for delays in the bottom-side ionosphere:

$$h_mF_2 = \frac{1490}{M(3000)F_2 + \Delta M} - 176 \quad \text{(km)} \quad (1)$$

$$\Delta M = \frac{0.18}{X_E - 1.4} \quad \text{for} \quad X_E > 1.7 \quad (2)$$

$$X_E = \frac{f_oF_2}{f_oE} \quad (3)$$

Berkey and Stonehocker[18] confirmed that this expression is sufficiently accurate when compared to the method of determining actual heights from whole echo traces by iterative computation. $M(3000)F_2$ as used here is one of the standard ionogram scaling parameters and can be established with relative ease, while the scaling whole echo traces involves huge amounts of labor and time. Because f_oE appearing in Equation (3) sometimes is unavailable under the influence of the sporadic E-layer or interference, the empirical equation developed by Muggleton[19] was used instead. Parameters of the E layer can be well defined in terms of the solar zenith angle and the solar activity index, and are less vulnerable to the effects of ionospheric storms.

4 Space Weather Event in Early November 2001

4.1 Overview of disturbances

Figure 3 shows the interplanetary magnetic field and geomagnetic variation parameters for November 5 to 8, 2001. The top panel designates the southward component of the interplanetary magnetic field as observed by the ACE satellite at the Lagrange (L1) point. Here, the trace is shifted by one hour to allow for the propagation time of solar wind from the L1 point to the earth. The two panels in the middle indicate the magnetic disturbance indices of ASYM-H and SYM-H[20]. The ASY-H index (an asymmetric disturbance index) is considered a good indicator of an auroral substorm. The SYM-H index (a symmetric disturbance index) is essentially identical to the D_{st} index, except that it has a high time resolution and uses somewhat different observatories to derive the index. The bottom panel indicates a third magnetic disturbance index—the K_p index. A magnetic storm designated as SC (storm sudden commencement) started at 01:51 UT on November 6, with asymmetric ring current growing immediately. The K_p index reached 9-maximum. During the 7-hr period prior to the sudden commence-

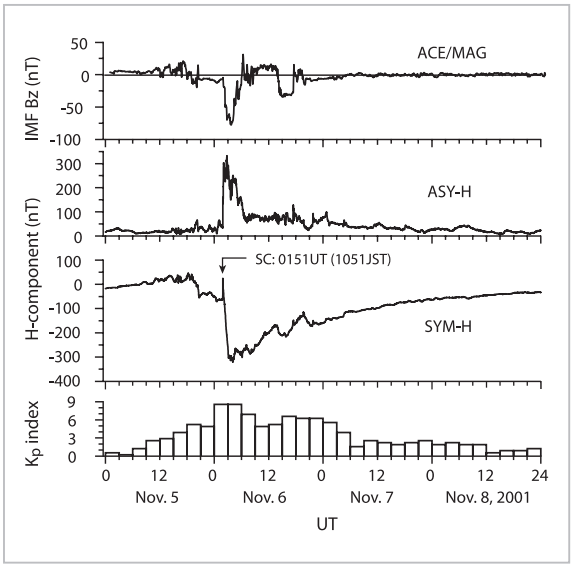

Fig.3 Magnetic disturbance index in early November 2001

ment of the magnetic storm, IMF Bz was southward, with the ring current growing gradually from 19:00 UT on November 5. In response to this, the K_p index increased from 3 to 5.

Figure 4 shows variations in N_mF_2 observed at the four stations from Wakkanai to Okinawa for November 2 to 7, along with the K_p index. Each dot denotes a value of N_mF_2 observed every 15 min; each solid line denotes an average value of N_mF_2 on quiet days. The average from November 2 to 4 was used as a quiet day reference. N_mF_2 was found to have disturbed at all the stations following the magnetic disturbance on November 6. Disturbances began with an increase in N_mF_2 at sunrise, soon followed by a reduction therein. At the lower latitude station, the earlier a reduction in N_mF_2 began by a larger amount. The N_mF_2 disturbances turned positive at 12:00 JST at the three lower-latitude stations, followed by Wakkanai turning positive at 13:30 JST. Thereafter, N_mF_2 remained higher than on quiet days until midnight at higher latitudes (Wakkanai and Kokubunji), while the N_mF_2 disturbance turned negative again at around 15:00 JST at lower latitudes (Yamagawa and Okinawa). In particular, N_mF_2 reduced noticeably at Okinawa and the reduction persisted until midnight. N_mF_2 began to change to a positive disturbance at 22:00 JST at Yagagawa and at 01:30 JST (on the following day) at Okinawa. In this way, the ionospheric disturbances observed in N_mF_2 are quite complicated in terms of both latitude and time, but showed rather small variation for the magnitude of magnetic storm, except during the evening at Okinawa.

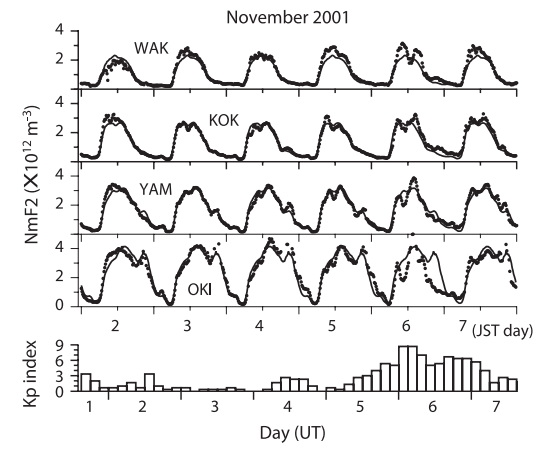

Fig.4 *Variations in the F-layer maximum electron density*

Figure 5 shows a map of time–latitude distributions of TEC. The top panel shows an average on quiet days from November 2 to 4 as in the case of N_mF_2, with each numeric value accompanying a contour line indicating TEC units (10^{16} electrons/m^2). TEC started increasing at sunrise and reached its maximum around noon at the northern end (45° N) and around 14:30 JST at the southern end (27° N). A second peak appeared at latitudes lower than 30° N after sunset as a consequence of the equatorial anomaly starting to develop again as driven by an increased $\mathbf{E}\times\mathbf{B}$ drift resulting from prereversal enhancement of the eastward electric field. The middle panel shows the distributions of TEC during the magnetic storm on November 6. Note the significantly marked increase in TEC in the daytime. TEC maximized at 13:45 JST at the southern end (27° N) and somewhat later at 14:15 to 14:30 JST at the northern end (45° N).

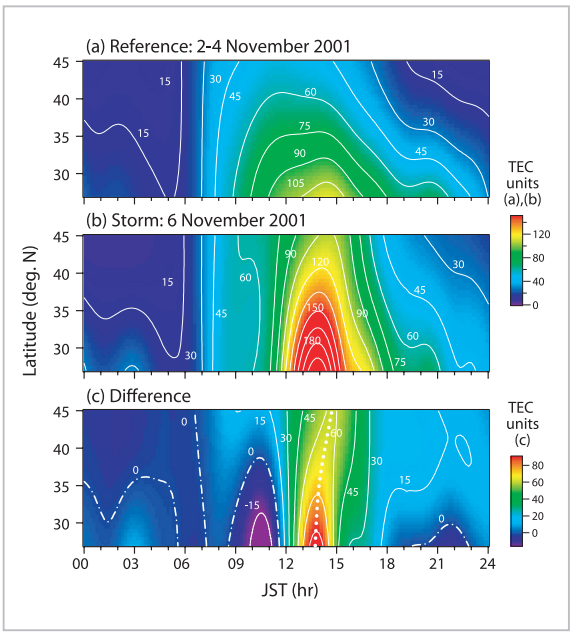

Fig.5 *TEC disturbances*
(a) Typical behavior on quiet days
(b) TEC storm observed on November 6, 2001
(c) Differences from quiet days

The difference (ΔTEC) map subtracting the map on quiet days from the TEC map on November 6 is given in the bottom panel to provide more evidence of the appearance of disturbances. The difference map not only evidently spots anomalous increases in TEC but also indicates that the increases started between 11:00 and 12:00 JST at about the same time at all latitudes. The time at which the increase in TEC peaked was found to shift toward a later time with latitude as denoted by the dotted line: It was 13:45 JST at the southern end and 14:45 JST at the northern end. At latitudes higher than about 33° N, a moderate positive disturbance lasted until midnight after the peak increase in TEC. Another fact revealed by the difference map is that the anomalous increase in TEC was preceded by a reduction in TEC at 09:00 to 11:30 JST at lower latitudes. The magnitude of this reduction was more pronounced in a lower-latitude region as in the case of the increase in TEC following it.

Since the TEC examined here is the quantity integrated along the radio wave propagation path from a GPS satellite to the ground, a greater contribution stems from the F-layer peak electron density height. Hence, the ways ionospheric storms are perceived in terms of N_mF_2 and TEC should be similar. The top two panels in Fig.6 compare the disturbance components of N_mF_2 and TEC from 12:00 JST on November 5 to 12:00 JST on November 7. At Wakkanai, ΔTEC and ΔN_mF_2 amid the large-scale disturbance gave fairly different looks against expectations. ΔTEC gradually increased from 06:00 JST on November 6, accelerated at 11:00 JST, and then peaked at 14:45 JST before decreasing at a monotonous rate. On the other hand, ΔN_mF_2 was found to peak moderately around 10:00 and 15:30 JST; between those peaks, it sagged to a negative value. Meanwhile, there was a rapid surge in ΔTEC during the same time period.

ΔTEC and ΔN_mF_2 at lower latitudes (Kokubunji, Yamagawa, and Okinawa) exhibited similar trends in variation from 09:00 to 15:00 JST. Both posted negative values around 10:30 JST, and positive values around 14:00 JST. When compared quantitatively, however, the two characteristics varied considerably in their amplitude of positive and negative variations. ΔTEC had significantly large positive variations (of about 100 TEC units observed at the latitude of Okinawa), but its negative variations were not so large (at about 20 TEC units observed at the latitude of Okinawa). In contrast, ΔN_mF_2 showed a positive range of variation equal to or smaller than the negative range of variation. Such a difference is more pronounced at lower latitudes. Another point worthy of mention regarding the difference between ΔTEC and ΔN_mF_2 is an extremely deep reduction in ΔN_mF_2 centering on 21:00 JST at the latitude of Okinawa, when compared with only a shallow drop in ΔTEC.

The ionospheric disturbance observed on November 6, 2001, was a most complex one. The goal of elucidating each of the underlying physical processes might not be easily attained by simply reviewing changes in N_mF_2 and TEC, but if variations in ionospheric height are analyzed in conjunction with those changes, a variety of processes would emerge into view. Figure 7 is mass plots of h_mF_2 daily variations observed at Kokubunji from November 2 to 6, during which the quiet days from November 2 to 5 are shown by thin solid lines, while the disturbance day of November 6 is designated by a thick solid line. Large day-to-day variations are found at nighttime, particularly from midnight to sunrise, but converged in a similar pattern in the daytime, except for the disturbance day. The ionospheric height started rising at about 11:00 on November 6 and reached a maximum difference of 100 km from the quiet days, maintaining that state until about midnight. Similar to TEC and N_mF_2, the values of Δh_mF_2 calculated by subtracting the quiet-day level from the disturbance day values are shown in the bottom panel of Fig.6. Figure 8 presents a sketch (O-mode only) of the ionograms (every hour) recorded at this time, with a continuous line designating the disturbance day and a dotted line marking the ionogram for the previous

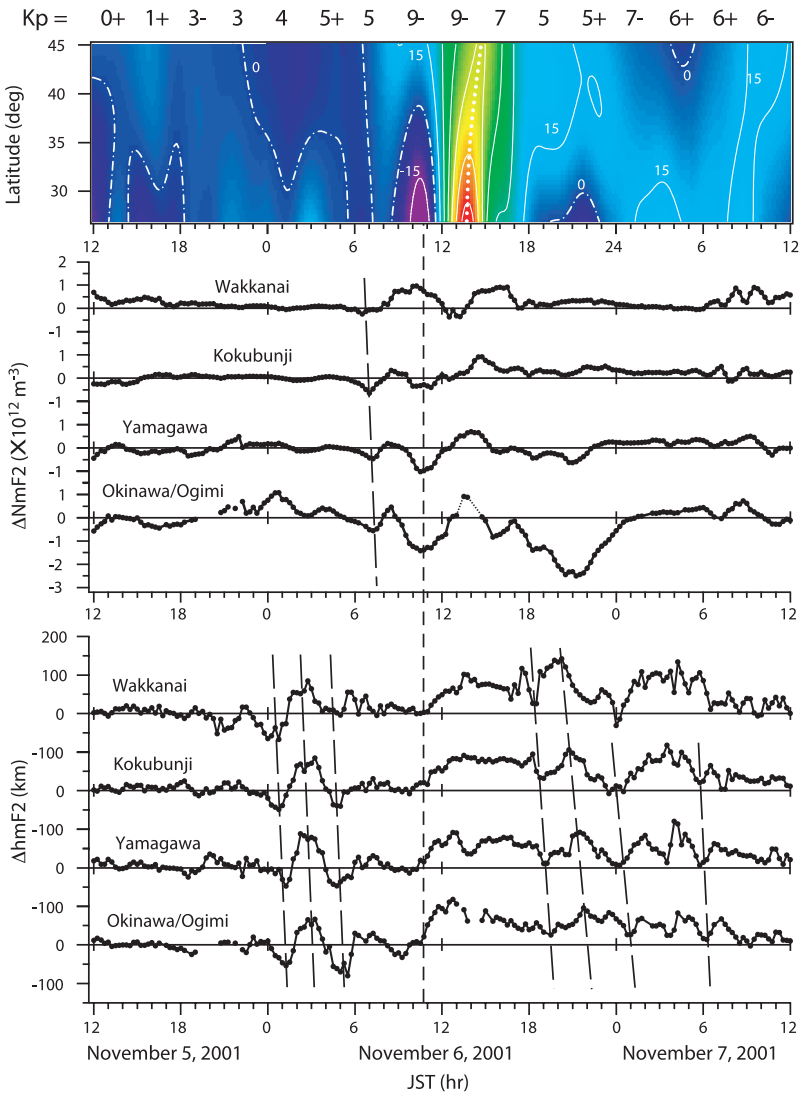

Fig.6 *Differences in TEC, F-layer maximum electron density, and F-layer height from their quiet-day averages*

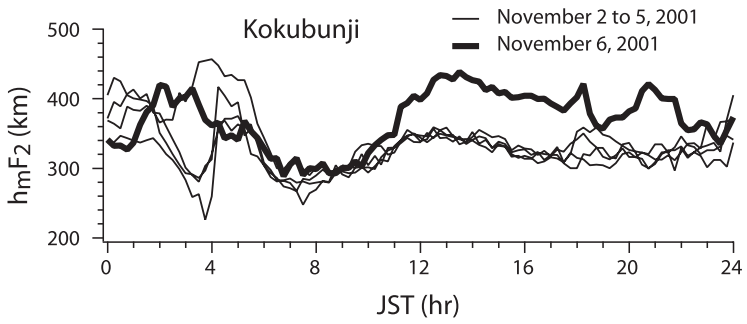

Fig.7 *Variations in the F-layer height on November 2 to 6, 2001*

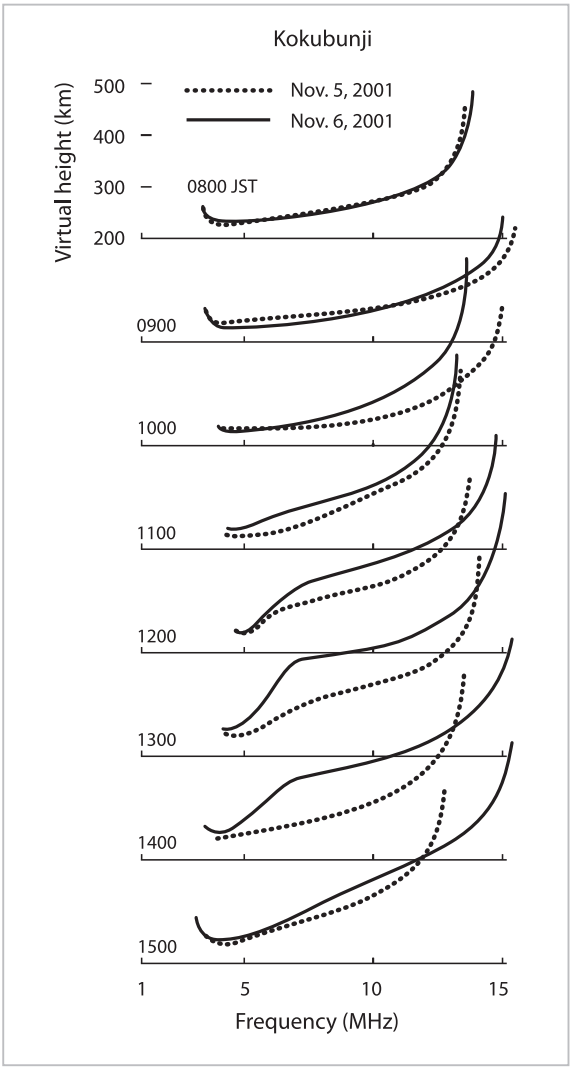

Fig.8 *Sketches of the ionogram for the TEC storm day and the previous day (O-mode only)*

day for the sake of comparison.

4.2 Discussions on the November 2001 event

The leading factor causing ionospheric disturbances should change from time to time during the storm event summarized in the previous section, which made the ionospheric storm appear so complex. Thus, we will discuss the storm mechanisms by dividing the period according to aspects of the disturbance.

4.2.1 Before 07:00 JST on November 6

According to Fig.6, TEC and N_mF_2 during this time period showed virtually no differences from the quiet days, but h_mF_2 significantly varied. Since Δh_mF_2 was found to have its phase shifted toward a later time at lower latitudes (as marked by an inclined long dashed line in the diagram), this disturbance may have been an effect of traveling ionospheric disturbances (TIDs). From the inclination of the dashed line, the velocity of propagation is estimated at 740 m/s—the velocity of a typical large-scale TID (LSTID). A similar TID was observed from 18:00 JST on November 6 to 06:00 JST on November 7, with an estimated velocity of propagation ranging from 350 to 700 m/s. Despite major variations in h_mF_2, there had been little disturbance to TEC and N_mF_2, which is characteristic of a nighttime TID. Generally, an ionosonde chain set up in a latitudinal direction, like the one used here, should provide very useful data to help distinguish between the effect of a TID as a source of change in h_mF_2 and an electric field or neutral atmospheric circulation effects.

4.2.2 From 07:00 to 11:00 JST on November 6

During this time period, IMF Bz turned southward while the K_p index exhibited a weak magnetic disturbance, as can be seen in Fig.3. The ionosphere shown in Fig.6 is characterized by a noticeably pronounced reduction in TEC at lower latitudes, with ΔTEC turning negative at latitudes lower than 38° N from 09:00 to 11:00 JST. In response to this drop in TEC, N_mF_2 decreased at Okinawa, Yamagawa and Kokubunji approximately 30 min later than ΔTEC. There was little height variation. Δh_mF_2 changed from a weak positive disturbance to a weak negative disturbance in Okinawa. The higher the latitude, the less distinct this trend appeared. In Fig.8, almost identical ionogram traces were seen at 08:00 on November 5 and 6, but at 09:00 on November 6 the height began to fall at lower frequencies, with f_oF_2 declining. One hour later, f_oF_2 further declined.

A summary review of comparisons of TEC, N_mF_2 (f_oF_2), and h_mF_2 reveals two conflicting ionospheric storm processes. An equatorial wind stirred a weak positive storm at

higher latitudes, while a transient negative storm driven by a westward electric field occurred at lower latitudes; both effects balanced near 38° N.

4.2.3 Extreme enhancement of TEC from 11:00 to 16:00 JST on November 6

Among the sequence of disturbances, the increase in TEC during this time period was most significant. TEC rose by 100 TEC units at the latitude of Okinawa during a period of 2 hours, and by 50 TEC units at the latitude of Wakkanai. The sharp rise in TEC appeared to start at the same time at all latitudes, but the time of their maximum came later at higher latitudes. Variations in N_mF_2 shown in the middle panel of Fig.6 were not so large when compared with noticeably large variations in TEC shown in the top panel. ΔN_mF_2 even had its sign changed. Rises in the F-layer height started at 11:00 JST simultaneously at all the stations, and coincided with the start of rising TEC as designated by the short-dashed line penetrating the middle through to the bottom panels. The rising height reached an equilibrium state in 2 hours and remained constant until the next day. The sources of these disturbances will be elucidated one by one.

Penetrating magnetospheric electric field

Simultaneous rises in ΔTEC and Δh_mF_2 at each latitude may well be understood as manifestations of a magnetospheric electric field penetrating the lower-latitude ionosphere (as reported in References[9][21]–[23]). IMF Bz was southward for 7 hours before the sudden commencement of the magnetic storm at 01:51 UT on November 6, with southward Bz intensifying around 02:00 UT and being accompanied by an increase in ASY-H. According to theoretical calculations by Spiro et al.[22], such penetrating electric field disturbance is eastward, which is consistent with the rising ionospheric height caused by the **E**×**B** drift observed. Low-latitude geomagnetic observation data also confirm the penetration of an eastward electric field[23].

The electric field strength can be estimated from the rate of rise in F-layer height and the geomagnetic inclination over Okinawa. From the slope of the curve for the 30-min period following the start of rising h_mF_2 in Fig.6, the rate of rise can be estimated at 28 m/s, which is an eastward electric field equivalent of 1.4 mV/m. This would be even more pronounced when considering the effect of induced descent of the F-layer along the geomagnetic field line by gravity[24].

Dissipation to the plasmasphere

The smaller change in N_mF_2 when compared with the increase in TEC might be caused by the dissipation of ionospheric plasma to the plasmasphere, thereby suppressing rises in the maximum electron density. A general solution that represents the equilibrium state of the plasma diffusion equation at heights above the F-layer peak can be stated in an equation as:

$$N = N_1 \mathrm{e}^{-(h-h_0)/2H} + N_2 \mathrm{e}^{-(h-h_0)/H} \quad (4)$$

where, N denotes the electron density at height h, and H the scale height of the neutral atmosphere. The first term on the right-hand side represents a diffusive equilibrium; the second term is a flux solution that designates deviation from the diffusive equilibrium[14]. In the intermediate region between the F-layer peak and $O^+ - H^+$ transition height, the plasma flux along the geomagnetic field line can be approximated as[14].

$$\Phi = \left(\frac{D_m}{2H}\right) N_2 \sin I \quad (5)$$

where, D_m denotes the diffusion coefficient of plasma at the F-layer peak and I the magnetic inclination. If the topside ionosphere is in a diffusive equilibrium, N_2 would equal 0, but normally there is an upward flux ($N_2 > 0$) in the daytime and a downward flux ($N_2 < 0$) in the nighttime through exchanges of plasma between the ionosphere and plasmasphere.

Assume that the ionospheric height is suddenly elevated 100 km in the daytime when N_2 is positive as shown in Figs.6 and 7. Because

this rise in height is greater than the scale height (~ 80 km) of the neutral atmosphere at the *F*-layer peak, the diffusion coefficient of the plasma appreciably increases by the decrease in ion-neutral collision frequency. As a result, the upward flux expressed by Equation (5) would increase by more than *e* times. A quantitative approach to this problem is detailed in another paper[25] in this special issue.

TEC enhancement

Consider the electron density at a given height in the bottomside ionosphere. If the ionosphere is suddenly uplifted, the electron density would initially fall sharply because the density gradient is upward on the bottomside. However, the electron density is soon compensated by the progress of an ionization process and it reaches a photo-chemical equilibrium. As a result, there is a resultant net increase in TEC. Compensation takes approximately $1/\beta$ to complete (with β being the recombination coefficient of electrons), which is about 10^3 s at a height of 250 km and 10^4 s at a height of 350 km. On the other hand, near the maximum electron density height, increases in density caused by a reduced loss rate conflict with the lowering density caused by an increased upward dissipative flux, which produces a delay of 2 to 3 hours (10^4 s) in the recovery of N_mF_2 despite a temporally (10^3 s) increase in TEC.

The process explained above is consistent with the hourly changes in the ionogram plotted in Fig.8. The *F*-layer height started rising at 11:00 JST and the trace began shifting upward. At this time, there was no increase in N_mF_2 (f_oF_2) yet. The trace continued to rise from 12:00 to 13:00 JST, while an intense effect of maintaining a photo-chemical equilibrium (compensating for the density loss due to upwelling) was found at work at lower altitudes (low frequency part of the ionogram). Folded segments below 7 MHz in the traces represent an F_1 layer, which normally does not appear distinctly at this time of the year. f_oF_2 also showed a distinct rise at 12:00 and then progressed at a high level. At 15:00 JST, compensation from the progress of the new ionization virtually pervaded the entire frequency range (at all altitudes), with f_oF_2 remaining at a high level. Since f_oF_2 starts declining during this time period on quiet days, the difference from the quiet days ΔN_mF_2 plotted in Fig.6 (for Kokubunji in the middle panel) is maximized.

Delay in the enhancement peak of TEC

The extreme enhancement in TEC has been attributed to the penetration of a magnetospheric electric field into lower latitudes. Such an electric field should work simultaneously at all latitudes. In fact, rises in the *F*-layer driven by the $\mathbf{E}\times\mathbf{B}$ drift began simultaneously as shown in the bottom panel of Fig.6. Yet, maximum of the enhancement in TEC tends to come later at higher latitudes as indicated by a dotted line in the bottom panel of Fig.5. At higher latitudes, the geomagnetic field line lengthens to penetrate a greater proportion of the plasmasphere. Consequently, the plasma takes longer to dissipate from the ionosphere to the plasmasphere, thereby possibly slowing down the rate of the increase in TEC.

4.2.4 Period of recovery from 16:00 JST to midnight

The aspect of recovery from the extreme enhancement of TEC to the quiet day level is clearly different at higher and lower latitudes across 33° N as can be seen in Fig.6. At lower latitudes, ΔTEC continued to decrease until 21:45 JST with a higher rate at lower latitude. Conversely, at higher latitudes, ΔTEC plummeted from 50 to 30 TEC units and kept a high level from 17:00 to 23:00 JST. The ionospheric height remained at a higher level than on quiet days at all latitudes as can be seen from Δh_mF_2 shown in the bottom panel in Fig.6, except for a superposition of a vertical fluctuation of TID. Therefore, at higher latitudes, the uplifting of the ionosphere by an equatorward wind may have suppressed electron loss along with the downward diffusion of plasmaspheric plasma stored in the daytime, allowing a high TEC level to be maintained.

Negative ΔTEC after sunset at lower latitudes was observed at 21:00–23:00 JST (bottom panel of Fig.5), somewhat later than the second peak as observed on quiet days caused by the prereversal enhancement of the electric field (top panel of Fig.5) (regrowth of the equatorial anomaly) in day-to-day TEC variations. The occurrence of negative ΔTEC might be caused by the development of a disturbance dynamo electric field[10] driven by a sequence of geomagnetic/thermospheric disturbances, which modulated the electric field during the time of the prereversal enhancement[26] to hasten the westward reversal. As the effect of the electric field around the prereversal enhancement is pronounced at lower latitudes[27], the negative storm effect of the disturbance dynamo electric field might overcome the positive storm effect of the equatorward neutral wind (which weakens with lowering latitudes). The more prominent negative storm in N_mF_2 rather than TEC reflects the latitude structure as explained in Fig.9. In the figure, negative disturbance is confined in the shaded region. The quantity N_mF_2 is a local value at the maximum electron density height (F-peak)

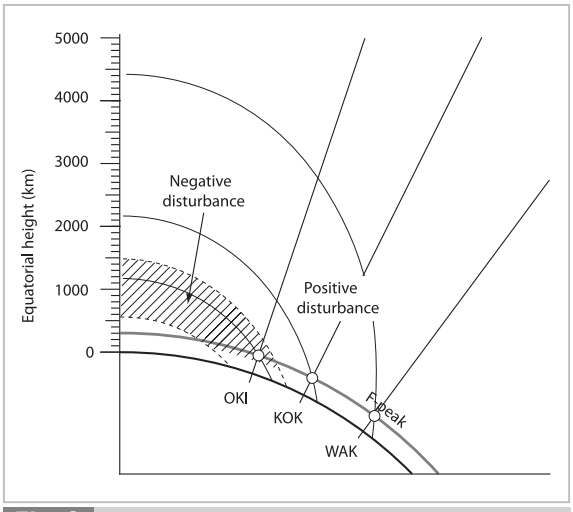

Fig.9 *Positive and negative phases of an ionospheric storm varying with latitude*

The positive storm at higher latitudes is caused by an uplift of ionospheric height due to an equatorward neutral wind, the negative storm at lower latitudes is caused by a receding fountain effect resulting from decay in the eastward electric field.

schematically represented in the figure, while the value of TEC is an integrated quantity along the vertical line. Magnetic field lines higher above the *F*-peak at low latitudes are connected to the *F*-peak at higher latitudes to extend the effect of positive storms in those regions.

4.2.5 After midnight

Both TEC and N_mF_2 no longer showed a major difference from their quiet day levels after midnight. As a general trend, the lower the latitude, the higher the value of ΔTEC, evidencing the effect of a disturbance dynamo electric field turning eastward at nighttime. Despite a larger value of Δh_mF_2 at a higher latitude, TEC continued to recover (dampen) to the quiet day level, probably under the influence of changes in the neutral atmospheric composition caused by a continuing southward circulation. In either case, the series of large disturbances came to an end.

5 Space Weather Event on November 8, 2004

5.1 Overview of disturbances

An intense magnetic storm occurred on November 7, 2004 during a declining phase of the solar activity cycle. Figure 10 plots IMF Bz (top panel) observed by the ACE satellite, the *AE* index (middle panel), and the D_{st} index (bottom panel). D_{st} started declining at 21:00 UT on November 7, when IMF turned southward and peaked at −373 nT at 06:00 UT. The vertical dotted line in the storm recovery phase designates the time at which the abnormal increase in TEC being discussed here was observed.

Figure 11 shows a map of time–latitude distribution of TEC variations. Dotted lines denote the times of sunrise and sunset at a height of 200 km. Here, Fig.11a represents the means for November 1 to 6 (JST) as typical quiet day variations; Fig.11b shows TEC variations on November 8 (when the disturbance was observed). The differences in ΔTEC between quiet and disturbance days are depict-

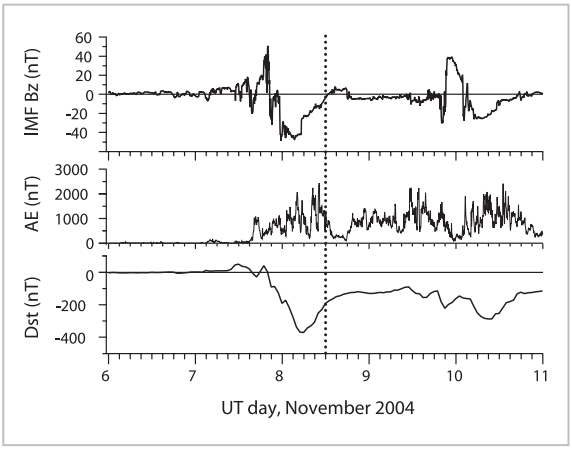

Fig.10 *Magnetic disturbance indices in early November 2004*

ed in Fig.11c. ΔTEC began to increase slowly a short while after sunrise and exhibited three major enhancements thereafter. The first of these enhancements was from 14:00 to 15:00 JST over the entire range of latitudes, with a slight delay in time at higher latitudes. The second one was observed from 17:00 to 19:00 JST around sunset and, unlike the first enhancement, was limited to a region lower than 37° N in latitude. The last one took place around 21:00 JST at latitudes higher than 35° N.

The TEC enhancement was associated with variations in *F*-layer height as in the previous event. Figure 12 shows variations in h_mF_2 observed at the four ionosonde stations for this event in 2004. Dots connected with a line denote a variation on the disturbance day (November 8) and the solid line is a mean variation on November 1 to 6, 2004 for reference. The letter "G" in the plots for Wakkanai and Kokubunji denotes that h_mF_2 is not calculated because the upper part of the trace exceeded the range of ionogram display due to a large propagation delay. A height rise took place around sunrise time (shown by an inverted open triangle) and remained high until past sunset (inverted filled triangle). The rise in the *F*-layer height at sunrise resulted in a moderate increase in ΔTEC; a large solar zenith angle right after sunrise might inhibit a sharp increase in TEC as noted in the 2001 event. The rising height began over Wakkanai at 04:00 JST and its onset time delayed with

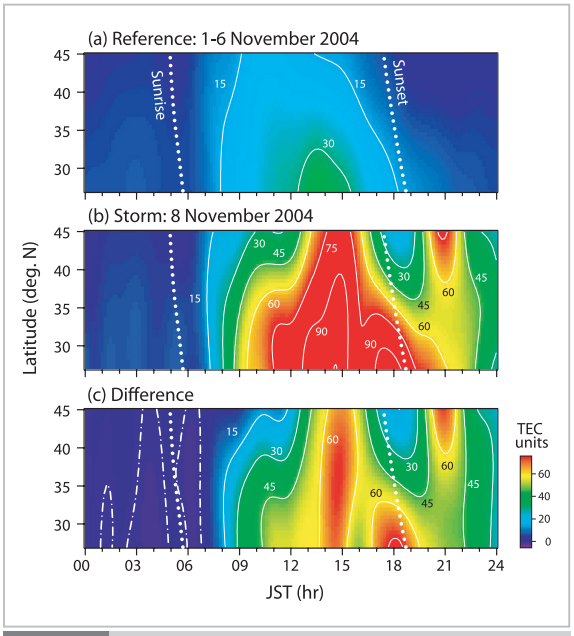

Fig.11 *TEC variations indicative of a TEC storm and SED*
(a) Typical behavior on quiet days
(b) TEC storm and SED observed on November 8, 2004
(c) Differences from quiet days

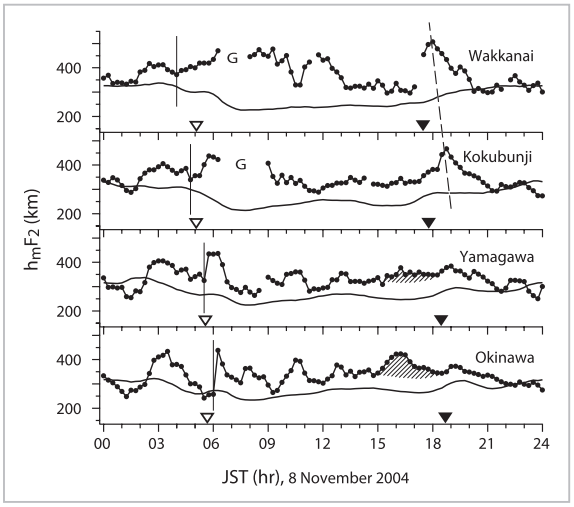

Fig.12 *Variations in the F-layer height observed at the four ionosonde stations*

Dots connected by a line denote a disturbance observed on November 8, 2004. The solid line designates a mean on quiet days from November 1 to 6, 2004.

decrease in latitude came at 06:00 JST over Okinawa. The leading edge of the rise appeared stepwise more distinctively at lower latitudes. This uplifting is not caused by an eastward electric field as described in the previous section, but by the effect of traveling

atmospheric disturbances (TADs) originating from a higher latitude or an equatorward surge[28].

The pronounced increase in TEC at 14:00−15:00 JST began sharply at about the same time, though the TEC peak at higher latitudes tended to delay. This is quite similar to the case discussed in the previous section, which is suggestive of the effect of **E**×**B** drift driven by a penetrating magnetospheric electric field, except for the different behavior of h_mF_2. The rise in h_mF_2 was not necessarily distinct in response to the rapid increase in TEC unlike the previous event. This may be due to an already intensified equatorward thermospheric wind having appreciably uplifted the *F*-layer, as well as a superposition of non-systematic and unidentifiable height fluctuation.

A gradual enhancement peak in h_mF_2 (shaded in Fig.12) was observed in Okinawa from 15:00 to 18:00 UT. This peak was barely noticeable in Yamagawa as well, but not in Kokubunji and Wakkanai. Obviously, this corresponds to the second upsurge in TEC at 18:00 JST. In Okinawa, TEC took about 3 hours to peak after h_mF_2 began to rise.

Lastly there was a prominent increase in TEC at 21:00 JST. A rising height characteristic of TID (a phase of variation delayed with lowering latitude) was observed during a slightly earlier time period as marked by the dotted line in Fig.12. Height variations observed at Wakkanai reverted to the quiet-day level by 20:15 JST, followed by a sharp increase in TEC. Because the rise in the *F*-layer height had occurred in a mid-latitude region after sunset, the source of TEC variations should obviously differ from the mechanism of positive storm occurrence as discussed in the previous section. This is ascribed to SED (storm enhanced density), which is rarely observed in Japan. The next section gives a detailed analysis of SED .

5.2 Storm Enhanced Density (SED)

Although Fig.11 gives the perspective of latitude distribution and temporal changes in ionospheric disturbances, TECs are average in the longitudinal direction across a number of cells with the same latitude. To examine spatial structure of SED in further depth, we chose cells aligned in the north-south direction at 141° E (cells 22, 23, 24, and 25 shown in Fig.13) and those aligned in the east-west direction at 41° N (cells 19, 24, and 28 shown in the same figure). The temporal variations in TEC for individual cells are plotted in Fig.14. A closer look at Fig.14a, which compares the north-south direction, reveals that TEC began rising after sunset as indicated by the dashed line, and then peaked at 20:30 JST at 43° N (cell 25). The increment in TEC during this period was 75 TEC units and the peak value larger than the value in the daytime at the same latitude. The lower the latitude, the later TEC began increasing and peaked, with a delay of 45 min at 37° N (cell 22). The lower the latitude, the less TEC increased, with 20 TEC units observed at 37° N. The apparent propagation velocity of the disturbance can be estimated at 8°/hr equatorward. A closer look at Fig.14b, which compares the east-west direction, reveals that the increase in TEC after sunset began earlier eastward, with an apparent propagation velocity of the distur-

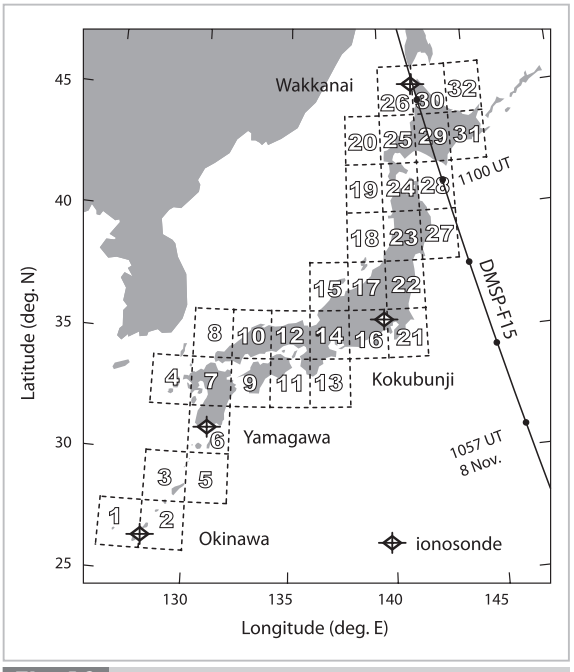

Fig.13 *Cells for which TECs were evaluated*

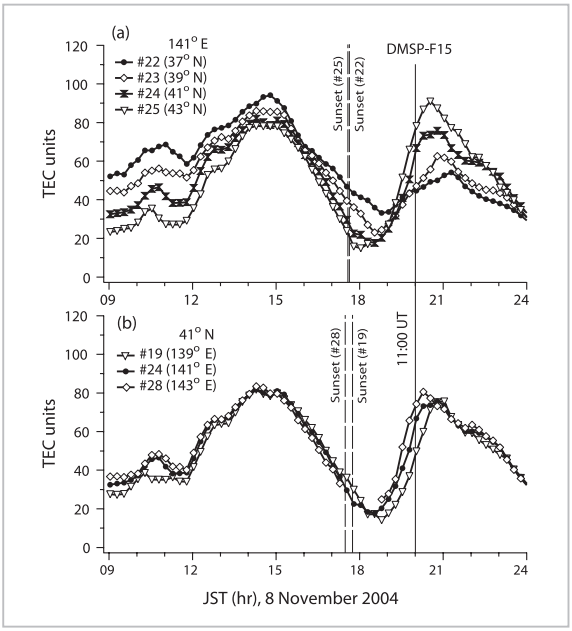

Fig. 14 *(a) TEC temporal variations in the north-south aligned cells (b) TEC temporal variations in the east-west aligned cells*

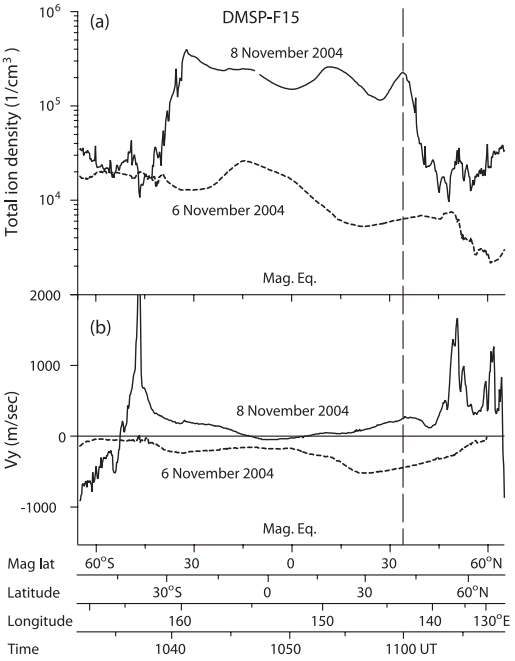

Fig. 15 *Total ion density and westward ion drift velocity observed by the DMSP satellite*

bance estimated at 8°/hr westward, which is roughly equivalent to half the solar terminator movement.

The TEC disturbance appearing to propagate equatorward strongly invokes a TAD originating from the auroral zone. Variations in the *F*-layer height observed around 18:00 JST at Wakkanai and Kokubunji exhibit a characteristic of a TAD. These variations are immediately followed by an increase in TEC of 53 TEC units an hour (cell 25). This is a flux equivalent of 10^{14} $m^{-2}s^{-1}$. At mid-latitudes with L ~ 1.5, the electron densities at the magnetic conjugate points are coupled with each other by H^+ flux along the magnetic field line[29]. If the increase in TEC observed here was caused by plasma flux from the opposite hemisphere, under the condition of the ionosphere being supported at a high altitude by a TAD, the H^+ field-aligned flux at the top of the ionosphere would be larger than the limiting flux[30] by two orders. Hence, it is difficult to ascribe the large increase in TEC to a TID induced by a TAD, and the effect of horizontal advection should be considered instead.

Figure 15a plots the total ion density at a height of 850 km as observed by the DMSP-F15 satellite. The solid line shows data recorded on November 8 (on the orbit shown in Fig.13) and the dashed line shows data recorded on November 6, a quiet day (on about the same orbit as for November 8) for the sake of comparison. The diagram should depict latitude changes, since this satellite is in a north-south sun-synchronous orbit (orbital inclination 98.4°). The ion density on November 8 was elevated from the level on quiet days over the entire latitude range, showing a density "bump" (at 41.1° N, 143.4° E; 11:00 UT; 20:00 JST) as marked by the long dashed line. If the increase in electron density (total ion density) had been induced by advection of **E×B** drift, the high-electron density structure should be aligned with the geomagnetic field line. When the position of the density enhancement at a height of 850 km observed by the DMSP-F15 satellite is projected onto the thin-shell height[15] of 400 km along the geomagnetic field line, it would be 43.5° N, 143.1° E, corresponding to cell number 29. TEC at 20:00 JST for cells 27 to 30 aligned south to north at 143° E was 54.7, 74.2, 95.7,

and 85.2 TEC units, respectively. Therefore, the density peak observed by the DMSP satellite and the TEC peak by the ground GPS network agree. In Fig.15a, another density enhanced region is noted at 19° N (12° N magnetic latitude) near the magnetic equator, corresponding to the location of the northern crest of the equatorial anomaly. This was not experienced on a quiet day and is suggestive of an intensified eastward electric field to promote the growth of the equatorial anomaly on November 8.

Figure 15b plots the westward ion drift velocity (a horizontal component perpendicular to the orbit) on the same orbit as in Fig.15a. The density enhanced region had velocity of ~ 250 m/s (or ~ 220 m/s when projected on the ground surface)—slightly faster than the velocity of the TEC frontal structure at 8°/hr (200 m/s). Since a northward drift velocity component of 40 m/s perpendicular to the geomagnetic field line was observed at the same time, the southward movement of the frontal structure of the TEC enhanced region was apparent, such that the actual movement of the density enhanced region is presumed to be a flow in the direction from ESE to WNW. Considering the fact that the apparent velocity of propagation of disturbances estimated from the TEC variations among the cells aligned in the north-south and east-west directions is 8°/hr both westward and equatorward, the behavior of the TEC enhanced region can be schematically depicted as shown in Fig.16. Such an extreme and localized density enhancement and the dynamics of the density-enhanced region are characteristic of SED. Furthermore, during this event, a westward high-speed plasma flow of the so-called SAPS (subauroral polarization stream) was observed at higher latitude by the DMSP satellite as shown in Fig.15b. SAPS is another characteristic closely related to SED/TEC plumes[31][32].

Previous studies[32]–[34] have revealed that SED/TEC plumes involve positive ionospheric storms at low latitudes resulting from development of the equatorial anomaly, but the equatorial anomaly and the density

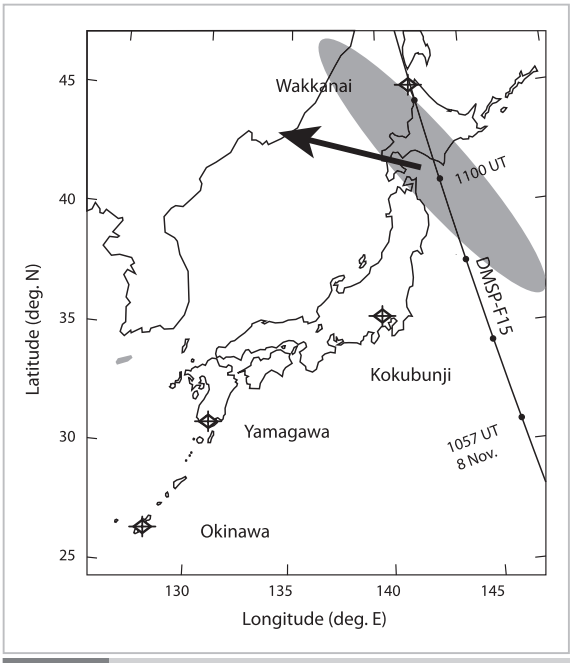

Fig.16 *Schematic illustration of SED observed on November 8, 2004*

enhanced region of SED appear to be separated by the relatively low density region between them. However, given the fact that high electron density at low latitudes caused by development of the equatorial anomaly accounts for the high electron density source of SED/TEC plumes, both regions are linked[33]. From this standpoint, the disturbances exemplified here may well be representative of a SED/TEC plume resulting from an intense TEC storm during the daytime.

Since the ion drift velocity of 250 m/s (or 220 m/s when projected on the ground surface) observed by the DMSP satellite in the density enhanced region was lower than the velocity of the solar terminator on the ground surface (400 m/s at 41° N), it follows that the density enhanced region had been formed to the east (and to the south) and at an early LT (local solar time). What should be noted about Fig.11 is that an increase in TEC was observed at lower latitudes at 18:00 JST, which corresponded to the uplift of the ionosphere at 15:00–18:00 JST. This is considered a consequence of the equatorial anomaly expanding to higher latitudes. The *F*-layer height was maximized at 16:00 JST, with

upward **E**×**B** drift being halted. The increase in TEC was maximized 2 hours later, which is in agreement with model calculations of height response to electric field changes[35]. Although the origin of the electric field disturbance occurring during this time period remains unclear, the equatorial anomaly expanding higher latitudes in the wake of the intense TEC storm in the daytime may have a close bearing on the formation of SED.

Another key factor involved in the formation of SED is the driving source for a sustained westward/poleward advection at mid- to low latitudes. The *F*-layer height remained high throughout the daytime as stated earlier, offering evidence of intensified equatorward thermospheric circulation. Such thermospheric wind disturbances set up a disturbance dynamo electric field. According to model calculations[10], a poleward electric field of 5 mV/m is produced all day long, along with an eastward electric field of 1 to 3 mV/m at a mid-latitude (41°) in the nighttime after 19:00 LT. These electric fields may provide a driving source for SED.

6 Conclusions

This article described two events in which extreme enhancement of ionospheric total electron content (TEC) —a key element of ionospheric space weather— was observed. The physical processes underlying the occurrence of these events were analyzed. One event is a TEC storm that occurred during the daytime; the other is SED (storm enhanced density) observed after sunset. Both events are the last stage of a sequence of space weather disturbances as schematically illustrated in Fig.17 and the largest TEC events ever recorded in the last solar cycle of 11 years (cycle 23) at Japan's longitudes. The reason for mentioning "Japan's longitudes" in particular is that the time at which magnetic disturbances occurred is very important as a source of driving ionospheric storms: Even a magnetic disturbance inducing a massive ionospheric disturbance in East Asia does not necessarily produce strong ionospheric disturbances at longitudes of the U.S. and vice versa. While ionospheric disturbances have a close bearing on

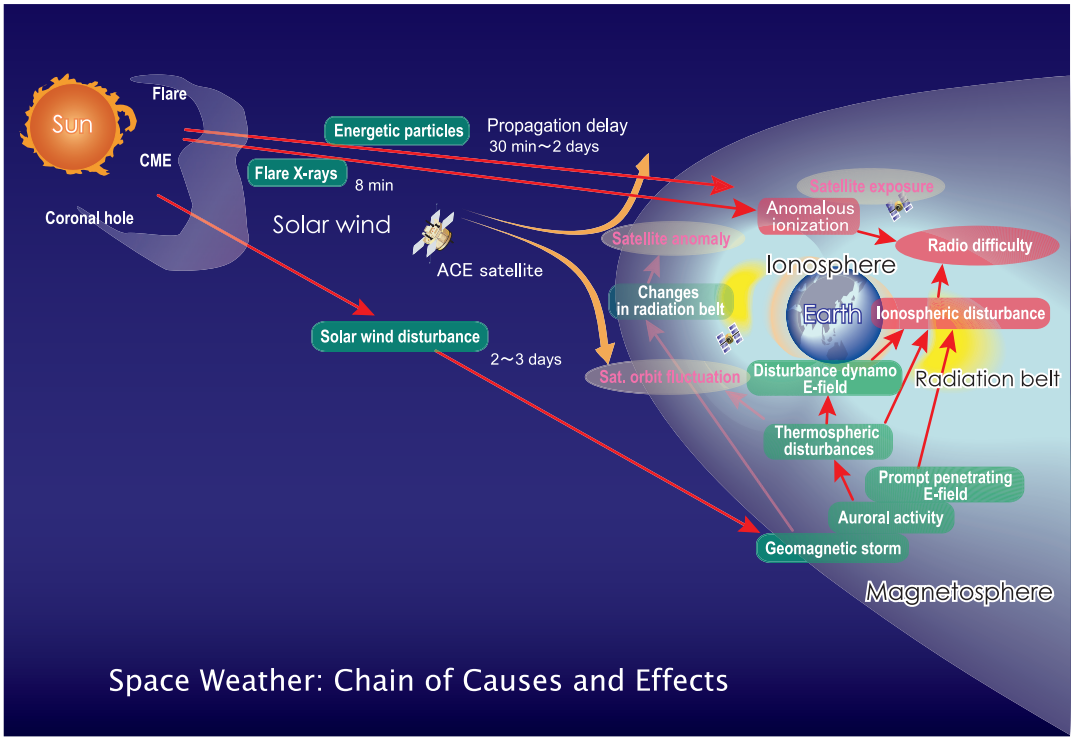

Fig.17 *Occurrence of radio wave propagation difficulty and origin of ionospheric disturbances*

longitude and time, whereas magnetic disturbances are a matter of the relation between the solar wind and the earth, with solar wind disturbances occurring independently of earth's existence. To be able to predict ionospheric disturbances occurring in a given longitudinal region on the earth from disturbances on the solar disk, a chain of "causes" and "effects" of disturbances as summarized in Fig.17 must be predicted with a time accuracy on the order of hours across the entire process flow. Simply being able to predict the occurrence of a magnetic storm would be far from reassuring as a means to forecasting radio wave propagation failures, because the ionospheric disturbance could become a positive or negative storm depending on the timing of its occurrence (see Reference[36] for the occurrence conditions of intense negative storms). As a practical solution to space weather prediction, developing a technique for predicting the passage of an ionospheric disturbance from its initial stages of occurrence onward would be valuable. To this end, in-depth post analyses as described in this paper should be indispensable.

Acknowledgments

GEONET was constructed and is maintained by the Geospatial Information Authority of Japan (GSI). We would like to thank GSI for the use of GEONET data.

References

1 D. Bilitza and B. W. Reinisch, "International Reference Ionosphere 2007: Improvements and new parameters," Adv. Space Res., Vol. 42, pp. 599–609, 2008.
2 T. Maruyama, "Regional reference total electron content model over Japan using solar EUV proxies," Special Issue of This NICT Journal, 3-3-5, 2009.
3 T. J. Fuller-Rowell, M. V. Codrescu, R. J. Moffett, and S. Quegan, "Response of the thermosphere and ionosphere to geomagnetic storms," J. Geophys. Res., Vol. 99, pp. 3893–3914, 1994.
4 T. J. Fuller-Rowell, M. V. Codrescu, H. Rishbeth, R. J. Moffett, and S. Quegan, "On the seasonal response of the thermosphere and ionosphere to geomagnetic storms," J. Geophys. Res., Vol. 101, pp. 2343–2353, 1996.
5 G. W. Prölss, "Ionospheric *F*-region storms," in Handbook of Atmospheric Electrodynamics, Vol. 2, edited by H. Volland, pp. 195–248, CRC Press, Boca Raton, Fla., 1995.
6 G. W. Prölss, "Magnetic storm associated perturbations of the upper atmosphere," in Magnetic Storms, Geophysical Monograph 98, edited by B. T. Tsurutani, W. D. Gonzales, Y. Kamide, and J. H. Arballo, American Geophysical Union, Washington, D.C., 1997.
7 M. J. Buonsanto, "Ionospheric storms – Review," Space Sci. Rev., Vol. 88, pp. 563–601, 1999.
8 G. W. Prölss, "Storm-induced changes in the thermospheric composition at middle latitudes," Planet. Space Sci., Vol. 35, pp. 807–811, 1987.
9 M. C. Kelley, B. G. Fejer, and C. A. Gonzales, "An explanation for anomalous equatorial ionospheric electric fields associated with a northward turning of the interplanetary magnetic field," Geophys. Res. Lett., Vol. 6, pp. 301–304, 1979.
10 M. Blanc and A. D. Richmond, "The ionospheric disturbance dynamo," J. Geophys. Res., Vol. 85, pp. 1669–1686, 1980.
11 B. G. Fejer, J. T. Emmert, G. G. Shepherd, and B. H. Solheim, "Average daytime *F* region disturbance neutral winds measured by UARS: Initial results," Geophys. Res. Lett., Vol. 27, pp. 1859–1862, 2000.
12 J. M. Forbes, M. Codrescu, and T. J. Hall, "On the utilization of ionosonde data to analyze the latitudinal penetration of ionospheric storm effects," Geophys. Res. Lett., Vol. 15, pp. 249–252, 1988.

13 J. M. Forbes, "Evidence for the equatorward penetration of electric fields, winds, and compositional effects in the Asian/Pacific sector during the September 17-24, 1984, ETS interval," J. Geophys. Res., Vol. 94, pp. 16,999–17,007, 1989.
14 H. Rishbeth, "On the F_2-layer continuity equation," J. Atmos. Terr. Phys., Vol. 48, pp. 511–519, 1986.
15 G. Ma and T. Maruyama, "Derivation of TEC and estimation of instrumental biases from GEONET in Japan," Ann. Geophys., Vol. 21, pp. 2083–2093, 2003.
16 T. Shimazaki, "World-wide daily variations in the height of the maximum electron density of the ionospheric F_2 layer," J. Radio Res. Labs., Vol. 2, pp. 85–97, 1955.
17 P. A. Bradley and J. R. Dudeney, "A simple model of the vertical distribution of electron concentration in the ionosphere," J. Atmos. Terr. Phys., Vol. 35, pp. 2131–2146, 1973.
18 F. T. Berkey and G. H. Stonehocker, "A comparison of the height of the maximum electron density of the F_2-layer from real height analysis and estimates based on $M(3000)F_2$," J. Atmos. Terr. Phys., Vol. 51, pp. 873–877, 1989.
19 L. M. Muggleton, "A method of predicting f_oE at any time and place," Telecommun. J., Vol. 42, pp. 413–418, 1975.
20 T. Iyemori and D. R. K. Rao, "Decay of the D_{st} field of geomagnetic disturbance after substorm onset and its implication to storm-substorm relation," Ann. Geophys., Vol. 14, pp. 608–618, 1996.
21 B. G. Fejer, C. A. Gonzales, D. T. Farley, M. C. Kelley, and R. F. Woodman, "Equatorial electric fields during magnetically disturbed conditions, 1. The effect of the interplanetary magnetic field," J. Geophys. Res., Vol. 84, pp. 5797–5802, 1979.
22 R. W. Spiro, R. A. Wolf, and B. G. Fejer, "Penetration of high-latitude-electric-field effects to low latitudes during SUNDIAL 1984," Ann. Geophys., Vol. 6, pp. 39–50, 1988.
23 T. Kikuchi, K. Hashimoto, and K. Nozaki, "Penetration of magnetospheric electric fields to the equator during a geomagnetic storm," J. Geophys. Res., Vol. 113, A06214, doi:10.1029/2007JA012028, 2008.
24 T. Maruyama, "$\mathbf{E}\times\mathbf{B}$ instability in the *F*-region at low- to midlatitudes," Planet. Space Sci., Vol. 38, pp. 273–285, 1990.
25 H. Jin and T. Maruyama, "Different behaviors of TEC and N_mF_2 observed during large geomagnetic storms," Special Issue of This NICT Journal, 3-3-2, 2009.
26 L. Scherliess and B. G. Fejer, "Storm time dependence of equatorial disturbance dynamo zonal electric fields," J. Geophys. Res., Vol. 102, pp. 24,037–24,046, 1997.
27 J. A. Murphy and R. A. Heelis, "Implications of the relationship between electromagnetic drift components at mid and low latitudes," Planet. Space Sci., Vol. 34, pp. 645–652, 1986.
28 G. W. Prölss, "On explaining the local time variation of ionospheric storm effects," Ann. Geophys., Vol. 11, pp. 1–9, 1993.
29 G. J. Bailey, P. A. Simmons, and R. J. Moffett, "Topside and interhemispheric ion flows in the mid-latitude plasmasphere," J. Atmos. Terr. Phys., Vol. 49, pp. 503–519, 1987.
30 P. G. Richards and D. G. Torr, "Seasonal, diurnal, and solar cyclical variations of the limiting H^+ flux in the earth's topside ionosphere," J. Geophys. Res., Vol. 90, No. A6, pp. 5261–5268, 1985.
31 J. C. Foster, P. J. Erickson, A. J. Coster, J. Goldstein, and F. J. Rich, "Ionospheric signatures of plasmaspheric tails," Geophys. Res. Lett., Vol. 29, doi:10.1029/2002GL015067, 2002.
32 J. C. Foster and W. Rideout, "Midlatitude TEC enhancements during the October 2003 superstorm," Geophys. Res. Lett., Vol. 32, L12S04, doi: 10.1029/2004GL021719, 2005.

33 J. C. Foster, “Storm time plasma transport at middle and high latitudes,” J. Geophys. Res., Vol. 98, No. A2, pp. 1675–1689, 1993.
34 M. Vlasov, M. C. Kelley, and H. Kil, “Analysis of ground-based and satellite observations of *F*-region behavior during the great magnetic storm of July 15, 2000,” J. Atmos. Solar-Terr. Phys., Vol. 65, pp. 1223–1234, 2003.
35 C. H. Lin, A. D. Richmond, R. A. Heelis, G. J. Bailey, G. Lu, J. Y. Liu, H. C. Yeh, and S. -Y. Su, “Theoretical study of the low- and midlatitude ionospheric electron density enhancement during the October 2003 superstorm: Relative importance of the neutral wind and the electric field,” J. Geophys. Res., Vol. 110, A12312, doi:10.1029/2005JA011304, 2005.
36 T. Maruyama and M. Nakamura, “Conditions for intense ionospheric storms expanding to lower-midlatitudes,” J. Geophys. Res., Vol. 112, A05310, doi:10.1029/2006JA012226, 2007.

***MARUYAMA Takashi**, Ph.D. (Eng.)*
Executive Researcher
Upper Atmospheric Physics

***MA Guanyi**, Ph.D.*
Professor, National Astronomical Observatories, Chinese Academy of Sciences.
Upper Atmospheric Physics, Satellite Communication and Navigation

***NAKAMURA Maho**, Ph.D.*
Expert Researcher, Space-Time Standards Group, New Generation Network Research Center
Ionosphere, Information Engineering